



## Construction of a high-resolution gridded rainfall dataset for Peru from 1981 to the present day


Cesar Aybar, Carlos Fernández, Adrian Huerta, Waldo Lavado, Fiorella Vega & Oscar Felipe-Obando

To cite this article: Cesar Aybar, Carlos Fernández, Adrian Huerta, Waldo Lavado, Fiorella Vega & Oscar Felipe-Obando (2020) Construction of a high-resolution gridded rainfall dataset for Peru from 1981 to the present day, Hydrological Sciences Journal, 65:5, 770-785, DOI: [10.1080/02626667.2019.1649411](https://doi.org/10.1080/02626667.2019.1649411)

To link to this article: <https://doi.org/10.1080/02626667.2019.1649411>

 View supplementary material [↗](#)

---

 Published online: 13 Aug 2019.

---

 Submit your article to this journal [↗](#)

---

 Article views: 6180

---

 View related articles [↗](#)

---

 View Crossmark data [↗](#)

---

 Citing articles: 48 View citing articles [↗](#)

---

# Construction of a high-resolution gridded rainfall dataset for Peru from 1981 to the present day

Cesar Aybar<sup>a</sup>, Carlos Fernández<sup>a,b</sup>, Adrian Huerta<sup>a</sup>, Waldo Lavado<sup>a</sup>, Fiorella Vega<sup>a</sup> and Oscar Felipe-Obando<sup>a</sup>

<sup>a</sup>Servicio de Meteorología e Hidrología del Perú (SENAMHI), Dirección de Hidrología, Lima, Perú; <sup>b</sup>Potsdam Institute for Climate Impact Research, Potsdam, Germany

## ABSTRACT

A new gridded rainfall dataset available for Peru is introduced, called PISCOp V2.1 (Peruvian Interpolated data of SENAMHI's Climatological and Hydrological Observations). PISCOp has been developed for the period 1981 to the present, with an average latency of eight weeks at 0.1° spatial resolution. The merging algorithm is based on geostatistical and deterministic interpolation methods including three different rainfall sources: (i) the national quality-controlled and infilled raingauge dataset, (ii) radar-gauge merged precipitation climatologies and (iii) the Climate Hazards Group Infrared Precipitation (CHIRP) estimates. The validation results suggest that precipitation estimates are acceptable showing the highest performance for the Pacific coast and the western flank of the Andes. Furthermore, a meticulous quality-control and gap-infilling procedure allowed us to reduce the formation of inhomogeneities (non-climatic breaks). The dataset is publicly available at <https://piscoprec.github.io/> and is intended to support hydrological studies and water management practices.

## ARTICLE HISTORY

Received 23 February 2019  
Accepted 21 June 2019

## EDITOR

A. Castellarin

## GUEST EDITOR

H. Lins

## KEYWORDS

quality control; gap-infilling; CHIRP; TRMM 2A25; quantile mapping; PISCOp V2.1

## 1 Introduction

Accurate spatio-temporal rainfall estimations are essential for the development of scientific and operational applications, which allow to understand the water cycle and its impact on natural and human systems. Conventional observations from raingauge stations are an ideal input for the aforementioned applications. Unfortunately, strong spatial variability (Garreaud *et al.* 2009) and the heterogeneous and sparse distribution of raingauges combined with systematic data quality deficiencies (Hunziker *et al.* 2017b) precludes their widespread use within Peru.

In the last decades, new algorithms based on the indirect estimations from advanced infrared and microwave satellites, have led to the construction of different gridded rainfall datasets (GRD) that are used as auxiliary data to overcome the lack of raingauge stations, increase the spatio-temporal resolution and reduce uncertainties in rainfall predictions (Baik *et al.* 2015, Verdin *et al.* 2015, Bi *et al.* 2017, Sun *et al.* 2017). GRD based on satellites have specific shortcomings in Peru. For instance, the TRMM Multi-satellite Precipitation Analysis (TMPA) 3B42 V7 (Huffman *et al.* 2007), the Climate Prediction Center MORPHing Technique (CMORPH, Joyce *et al.* 2004) and the Precipitation Estimation from Remotely Sensed Information using Artificial Neural Networks (PERSIANN, Sorooshian *et al.* 2000) tend to have large sensor errors over the Peruvian Andes (Derin *et al.* 2016), overestimate the magnitude of precipitation on the Pacific Coast (Ochoa *et al.* 2014) and span a short time period ( $\leq 20$  years). On the other hand, reanalysis-based GRD, e.g. the National Centers for

Environmental Prediction – Climate Forecast System Reanalysis (NCEP CFSR; Saha *et al.* 2010), tend to be of coarser spatial resolution and show lower performance than satellite products. However, GRD based on a blend of satellite, reanalysis and gauge rainfall sources are available. The most recent blended GRDs, with global and near real-time coverage, are the Multi-Source Weighted-Ensemble Precipitation (MSWEP; Beck *et al.* 2019) and the Climate Hazards Group Infrared Precipitation with Stations (CHIRPS; Funk *et al.* 2015a).

The MSWEP provides three-hour precipitation at a spatial resolution of  $\sim 10$  km for the period 1979 to the present, while CHIRPS covers daily precipitation at  $\sim 5$  km for 1981–present. Only a few studies have been done to analyse the performance of these new blended GRDs in adjacent regions of Peru. For instance, Zambrano-Bigiarini *et al.* (2017) show that both CHIRPS and MSWEP perform well at high temporal scales, presenting problems of overestimation (underestimation) in events of light rain (extreme rain) in Chile, whereas Perdigón-Morales *et al.* (2017) and Javier *et al.* (2016) mention that CHIRPS is acceptable at reproducing climatological values of monthly accumulated precipitation in Mexico and Venezuela, respectively. Nonetheless, these studies re-used raingauges that had been incorporated previously in the merging algorithm, which alters the reliability of blended GRD performance results. In line with this, Beck *et al.* (2017b) reported that MSWEP performs better than CHIRPS only in regions with extensive raingauge networks (e.g. in temperate regions). However, these findings cannot be directly applied to regions with sparse and irregular monitoring networks, such as Peru.

Recently, several studies have indicated essential considerations when generating daily and monthly blended GRD in data-scarce regions: (a) the efficiency of blended GRDs largely depends on the predictor, and the interpolation method used must be able to adapt to scenarios with high spatial heterogeneity (Dinku *et al.* 2014); (b) geostatistical interpolation methods outperformed deterministic methods at annual and monthly time steps, whereas for the daily time step, geostatistic and deterministic methods were proven to be comparable (Ly *et al.* 2013); (c) there are difficulties in assuming the space-stationary hypothesis and to establish an adequate theoretical semivariogram at the daily time step (Nerini *et al.* 2015); (d) the optimized interpolation parameters in deterministic methods significantly improve the final results (Chen and Liu 2012); (e) the gap-infilling in precipitation time series is highly important to minimize inhomogeneities in the gridded datasets for periods of missing data, especially in heterogeneous regions (Peterson *et al.* 1998, Begueria *et al.* 2015, Yanto *et al.* 2017); and (f) the use of simple ratios based on very high rainfall climatologies can significantly decrease the systematic bias (Strauch *et al.* 2016).

On this basis, this study presents the development of PISCOp V2.1, a new local blended GRD, headed by the National Service of Meteorology and Hydrology of Peru (SENAMHI). PISCOp V.2.1 contains daily and monthly rainfall grids at 0.1° computed for 1981–2019 covering the whole of Peru with an average latency of eight weeks. It is built using serially complete raingauge datasets, CHIRP V2.0 (without raingauge stations), radar-gauge merged precipitation climatologies, geostatistics and deterministic interpolation methods, and a simple monthly correction factor applied to daily estimates. The objective of this paper is to provide

detailed and transparent information about the construction of PISCOp V2.1 as well as to evaluate its performance and stress its limitations.

## 2 Material and methods

### 2.1 Study area

Peru is located in the central-western region of South America (0°–18°S; 68°–82°W) (Fig. 1), covering climatically extremely variable regions with diverse precipitation regimes that result from the interaction between synoptic-scale atmospheric currents, the complex orography of the Andes, the cold Humboldt Current System (HCS) and the El Niño Southern Oscillation (ENSO; Garreaud *et al.* 2009, Lavado Casimiro *et al.* 2012).

In the austral summer, easterly trade winds from the southerly position of the Intertropical Convergence Zone (ITCZ) transport humid air masses from the tropical Atlantic towards the Amazon Basin (Carvalho *et al.* 2011, Marengo *et al.* 2012, Manz *et al.* 2017) and to the south along the Andes through the South American Low-Level Jet (SALLJ; Vera *et al.* 2006, Boers *et al.* 2013). This period determines a marked wet season in most of Peru (Marengo *et al.* 2012). Conversely, when the ITCZ is located further north (austral winter), convection and, consequently, precipitation levels are significantly reduced.

In the Peruvian Andes, the climate is complex and primarily controlled by orography that acts as a topographic barrier to moisture flow, causing the formation of strong precipitation gradients on the eastern flanks of the Andes (Bookhagen and Strecker 2008). The inter-Andean valleys (> ~500 mm/year)

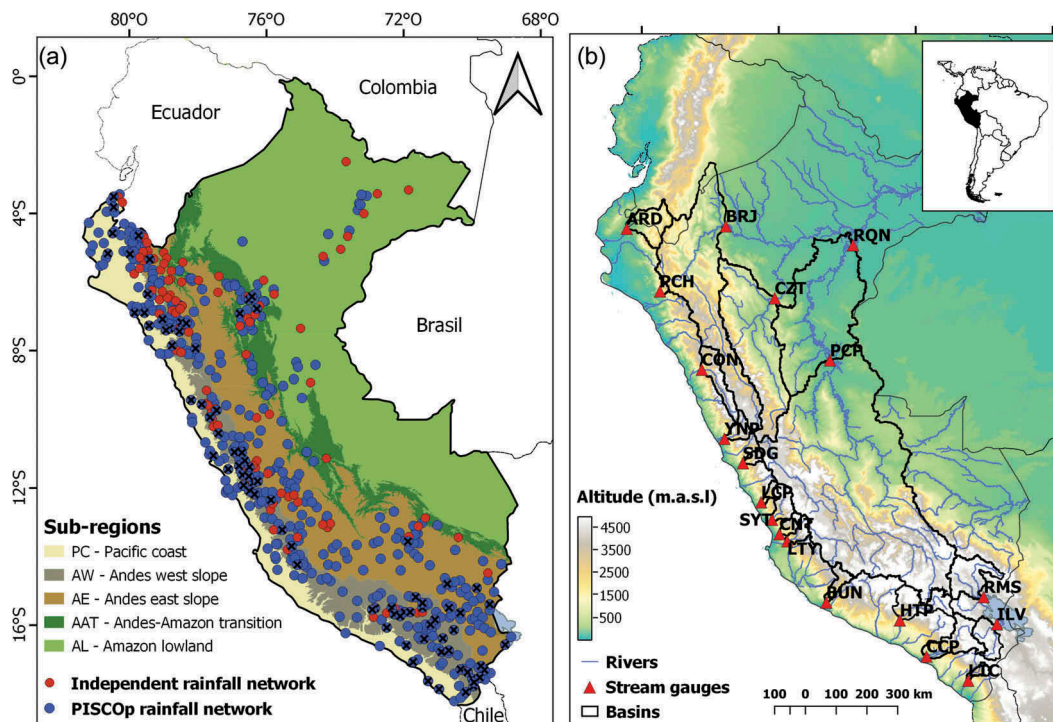


**Figure 1.** (a) Spatial extent of PISCOp V2.1. Points with × indicate stations with more than 95% of data within the 1981–2016 period. (b) Location and upstream catchments of the selected stream gauges.

are principally dominated by convective processes (Garreaud 1999, Campozano *et al.* 2016) channelling moisture intrusions of the Amazon (Chavez and Takahashi 2017). At the same time, the influence of cold and dry air masses originating from the HCS cause the driest conditions of our study area at the Pacific coast and on the western flanks of the Andes (< ~500 mm/year). However, during the occurrence of ENSO, the HCS weakens and the formation of severe convective storms can occur, especially over the northern Pacific coast (Antico 2009).

Based on the hydro-climatic heterogeneity described above and according to the classification of Manz *et al.* (2017), the study area was divided into five sub-regions (Fig. 1(a) and Table 1): (a) The Pacific coast (PC, average annual precipitation of ~150 mm/year); (b) The western Andean slopes (AW, ~400 mm/year), (c) the eastern Andean slopes (AE, ~1100 mm/year), (d) the Andes-Amazon transition (AAT, ~3200 mm/year) and (e) the Amazon lowlands (AL, ~2250 mm/year).

## 2.2 Raingauge dataset

The raw gauge dataset comprised 945 daily observation data provided by SENAMHI. The raingauge data spans the period 1981–2019 and is characterized by a high number of missing values and numerous quality issues (Hunziker *et al.* 2017b), being generally caused by the observer at the time of data collection (e.g. incorrect measurement of values  $\leq 1$  mm) and instrumentation malfunction. Even though metadata information would help to perform the data quality control, this was not used because of its limited availability. Therefore, our analysis of raingauge data mainly focused on gross error detection and gap-infilling methods.

### 2.2.1 Quality control (QC)

Most methods for quality control (QC) in raingauge observations are designed for dense station networks (Vicente-Serrano *et al.* 2010, Isotta *et al.* 2014, Notivoli *et al.* 2017), which are difficult to assume in this study. As expected, assuring the quality of a dataset is more problematic for data-scarce regions due to the reduced number of neighbouring stations (Hunziker *et al.* 2017b). Considering this fact and the lack of an established quality management system in Peru, we propose a three-step QC approach which can be considered

as conservative because only gross errors are deleted if there is strong evidence for implausibility. Hence, it is still expected to find some remaining errors after QC, especially in areas with a lower density of gauges. The following checks were applied:

- (1) General problems (automatic): to delete obvious inconsistent values, such as negative and non-physical precipitation, decimal point-related errors, repetitive dates, repetitive consecutive values and unexpected changes in latitude and longitude coordinates.
- (2) Spatial extreme values (automatic): a threshold of 200 years of return period of precipitation is used for the detection of extreme events, as in Keller *et al.* (2015). Then, if the extreme values occur in at least two neighbouring (<50 km) gauges for the same date, they are preserved, otherwise they are deleted.
- (3) Break and bad segments (manual): a visual control to recognize segments with asymmetric rounding patterns and obvious inhomogeneities.

### 2.2.2 Gap-infilling

Another source of uncertainty is found in the temporally inconsistent gauge network which is liable to produce systematic bias during the merging phase (New *et al.* 2000). This is of primary importance in data-scarce regions, where several raingauges come in and out of use (Hunziker *et al.* 2017b). Similar to the QC approach, there is no established methodology for gap-infilling in Peru. Therefore, we propose a two-step approach to generate a serially complete raingauge dataset.

First, relying on neighbouring gauges, the relatively newer and effective spatio-temporal imputation method, CUTOFF (Feng *et al.* 2014), was applied to infill the previously quality controlled gauge datasets at daily and monthly time steps. This method, unlike iterative imputation approaches (e.g. missforest, Stekhoven and Bühlmann 2012) or matrix decomposition techniques (Lindstr *et al.* 2013), is principally designed to handle missing values in raingauges by taking into account the spatio-temporal rain distribution. Before CUTOFF is applied, each raingauge is grouped with other raingauges if the following conditions are met: (a) distance < 100 km, (b) sharing a minimum of 10 years of data, and (c) daily (monthly) linear relationship > 0.5 (> 0.8). Secondly, if the previous condition is neither fulfilled nor enough to create serially complete time series, the quantile mapping bias correction (Qm), produced by matching the empirical cumulative distribution of the collocated grid cell (CHIRPm, see Section 2.3) to the available gauge data (Gudmundsson *et al.* 2012), is used to infill the remaining gaps of each raingauge.

## 2.3 Modification of CHIRP (CHIRPm)

CHIRP products at the monthly (CHIRP<sub>m</sub>) and daily (CHIRP<sub>d</sub>) time step are initially calculated from the preliminary pentad time-step product (CHIRP<sub>pentad</sub>) using the following equations (Funk *et al.* 2015a):

**Table 1.** Sub-regions defined for the analysis of PISCOp V.2.1. Adapted from (Manz *et al.* 2016), *N* is the number of raingauges within each sub-region.

Sub-region	Elevation (m a.s.l.)	Climate driver	Rainfall regime	<i>N</i>
Peruvian Pacific Coast, PC	0–1500	ITCZ, HCS, ENOS	Wet (Dec.–May) Dry (Jun.–Nov.)	97
Andes western slope, AW	>1500	Elevation, ITCZ	Wet (Dec.–May) Dry (Jun.–Nov.)	151
Andes eastern slope, AE	>1500	Elevation, Orography, ITCZ	Weak seasonality, drier JJA	128
Andes-Amazon transition, AAT	500–1500	Orography, ITCZ, SALLJ	Weak seasonality, drier JJA	26
Amazon lowland, AL	0–500	ITCZ, trade winds	Weak seasonality, drier JJA	39



$$\text{IRP}_{\text{pentad}} = b_0 + b_1 * (\text{TIR CCD}_{\text{pentad}}\%) \quad (1)$$

$$\text{CHIRP}_{\text{pentad}} = \text{CHP}_{\text{clim}} * \frac{\text{IRP}_{\text{pentad}}}{\text{IRP}_{\text{clim}}} \quad (2)$$

where  $\text{IRP}_{\text{pentad}}$  is the precipitation calculated from the linear model between thermal infrared cold cloud duration percentage (TIR CCD%) and TRMM 3B42 V7 product;  $\text{CHP}_{\text{clim}}$  are the monthly precipitation climatologies generated by Funk *et al.* (2015b) and  $\text{IRP}_{\text{clim}}$  represents the climatology of infrared precipitation.

Even though the use of climatic or monthly correction factors can reduce the systematic bias (Funk *et al.* 2015a, Keller *et al.* 2015, Parmentier *et al.* 2015, Strauch *et al.* 2016, Beck *et al.* 2017a, van Osnabrugge *et al.* 2017), it is crucial that the predictor of larger temporary aggregations (e.g.  $\text{CHP}_{\text{clim}}$ ) is well represented, otherwise a reverse process could occur. For Peru, we found that  $\text{CHP}_{\text{clim}}$  extremely overestimates precipitation (>500%) at the Peruvian coast between 8°–18°S (see Supplementary material, Fig. S1). Furthermore, it does not adequately represent the orographic rainfall hotspots over the Andes-Amazon transition and considers raingauges with poor reliability. Based on this,  $\text{CHP}_{\text{clim}}$  was replaced by our own climatology  $\text{PISCOp}_{\text{clim}}$  (see Section 2.3.1), resulting in the modified form of CHIRP, CHIRPM):

$$\text{CHIRPM}_m = \text{CHIRP}_m * \frac{\text{PISCOp}_{\text{clim}} + \varepsilon}{\text{CHP}_{\text{clim}} + \varepsilon} \quad (3)$$

$$\text{CHIRPM}_d = \text{CHIRP}_d * \frac{\text{PISCOp}_{\text{clim}} + \varepsilon}{\text{CHP}_{\text{clim}} + \varepsilon} \quad (4)$$

where  $\varepsilon$  is a threshold defined as 0.5 in the denominator and the numerator in order to deal with values of zero or near zero. This equation is applied to monthly and daily CHIRP estimates, resulting in  $\text{CHIRPM}_m$  and  $\text{CHIRPM}_d$ , respectively. CHIRP was previously resampled to a spatial resolution of 0.1 ° through cubic spline interpolation.

### 2.3.1 PISCOp climatology ( $\text{PISCOp}_{\text{clim}}$ )

For Peru it has been found that the TRMM precipitation radar product 2A25 (TPR; Iguchi *et al.* 2000) is the most suitable rainfall data source for identifying spatial precipitation variability and seasonal patterns, even for the complex orographic rainfall hotspots located in the eastern Andes (Bookhagen and Strecker 2008, Nesbitt and Anders 2009, Manz *et al.* 2016). Based on this dataset, we constructed monthly climatologies at 0.1° spatial resolution. The TPR data used corresponds to the 1998–2013 period, excluding the year 2014 because during that year the satellite was carrying out anomalous manoeuvres related to its dismantling (Houze *et al.* 2015). The construction procedure of  $\text{PISCOp}_{\text{clim}}$  (Fig. 2) is summarized as follows:

- (1) Extraction of suspicious pixels with a rain rate > 300 mm/h (Hamada and Takayabu 2014).
- (2) Aggregation of the entire TPR dataset to mean climatology estimates for each calendar month considering

the delineation of the overpassing TPR pixel, proposed by Manz *et al.* (2016).

- (3) Application of a spatial bias thresholding filter to replace the pixels with large ratios (>5 median) by the average of the surrounding 3 × 3 kernel.
- (4) Smoothing of rain rate through cubic spline interpolation.
- (5) Merging with the long-term (1981–2010) monthly climatologies raingauge dataset (Fig. 1(a)) using residual ordinary kriging (ROK, Section 2.4.2).

## 2.4 Merging phase of PISCOp V.2.1

The merging phase (Fig. 2) can be divided into four steps. Firstly, the provisional product P-PISCOp<sub>d</sub> is created by merging  $\text{CHIRPM}_d$  and serially complete daily gauge datasets applying residual inverse distance weighting (RIDW). Secondly,  $\text{PISCOp}_m$  is estimated by merging  $\text{CHIRPM}_m$  and completed monthly gauge datasets using ROK. Thirdly, a monthly correction factor (Mcf) is derived from the comparison of  $\text{PISCOp}_m$  and P-PISCOp<sub>d</sub> aggregated at a monthly time step. Finally,  $\text{PISCOp}_d$  is estimated by multiplying Mcf by P-PISCOp<sub>d</sub>.

### 2.4.1 Residual inverse distance weighting (RIDW)

Residual inverse distance weighting is used to generate P-PISCOp<sub>d</sub>. In this deterministic prediction method, the residuals are defined in each gauged location  $s_i$ , as follows:

$$r_o(s_i) = X_B(s_i) - X_O(s_i) \quad (5)$$

$$S_i \in S, i = 1, \dots, N \quad (6)$$

where  $N$  is the number of gauge observations,  $r_o$  are the residuals,  $X_O$  is the daily raingauge value and  $X_B$  is the  $\text{CHIRPM}_d$  value computed at each gauge location. The collocation of a raingauge to each  $\text{CHIRPM}_d$  grid cell was performed using the smoothed merging (SM; Li and Shao 2010) approach. Unlike centre neighbour approximation, SM operates over a 2 × 2 kernel considering the distances to the pixel centroids as weights, resulting in a smoothed field that reduces the boundary bias. To estimate the residual field ( $\mu_j$ ),  $r_o$  is interpolated by IDW at each grid point ( $j = 1, \dots, M$ ), given by:

$$\mu_j = \begin{cases} \frac{\sum_{i=1}^N w_i (||S_j - S_i||)^{r_o(s_i)}}{\sum_{i=1}^N w_i (||S_j - S_i||)} & \text{if } ||S_j - S_i|| \neq 0 \\ u_i & \text{if } ||S_j - S_i|| = 0 \end{cases} \quad (7)$$

$$w_i (||S_j - S_i||) = \frac{1}{||S_j - S_i||^\alpha} \quad (8)$$

where  $||\cdot||$  is the euclidean distance,  $w_i$  is the weight assigned to the gauge observation  $s_i$  and  $\alpha$  is the power parameter. The  $\alpha$  parameter controls the desired smoothness and the local behaviour in the spatial prediction. High (low) values of  $\alpha$  increase (decrease) the influence of the furthest observations, generating low (high) variance in the residual field. For additional details on IDW, see Babak and Deutsch (2009).

Different studies have examined the effects of varying  $\alpha$  for the spatial prediction of rainfall (Chen and Liu 2012, Adhikary 2017). Accordingly, the optimal  $\alpha$  was estimated

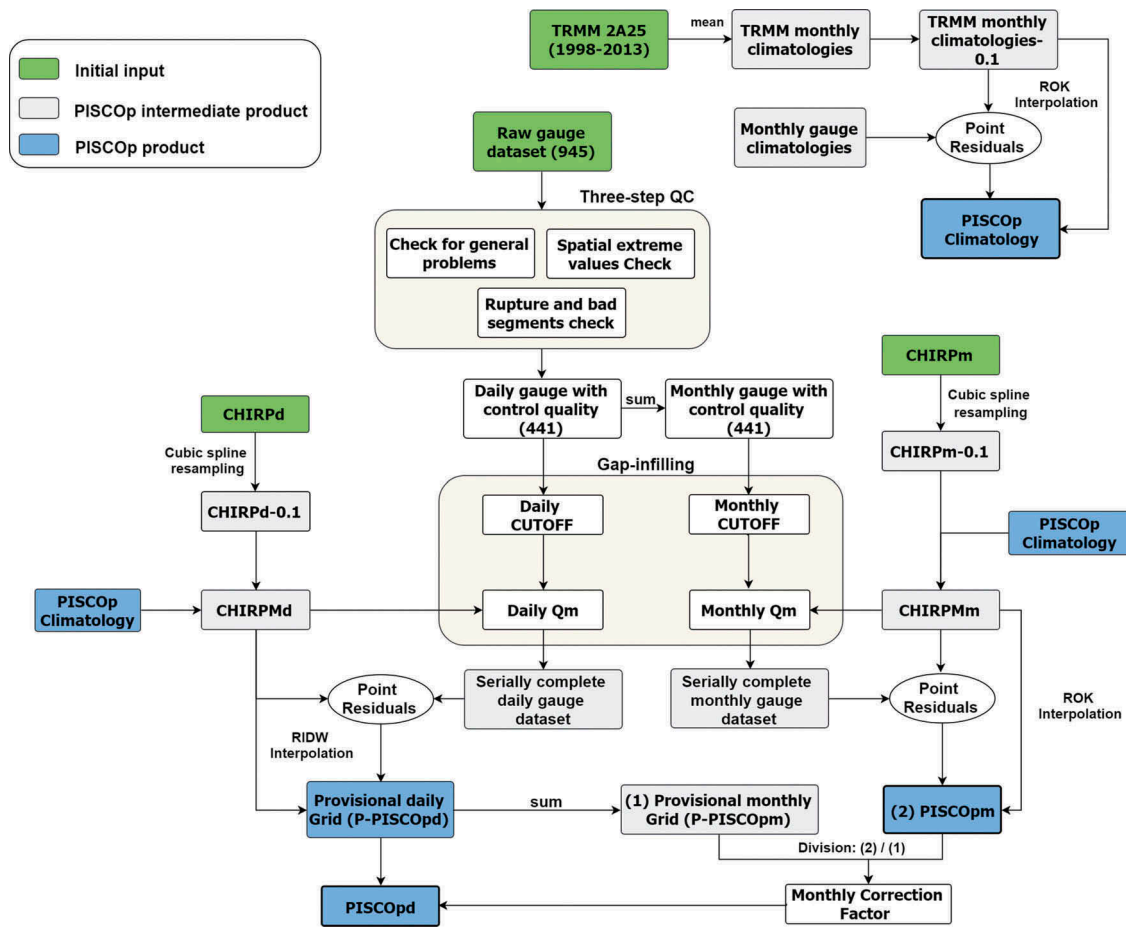


Figure 2. Schematic overview of the development of PISCOp V2.1.

by minimizing the root mean square error (RMSE) obtained from the 10-fold cross-validation. Finally,  $P\text{-PISCOp}_d$  is defined as:

$$P\text{-PISCOp}_d = \text{CHIRPM}_d - \mu \quad (9)$$

#### 2.4.2 Residual ordinary kriging (ROK)

Residual ordinary kriging is used for the generation of  $\text{PISCOp}_m$ . Similar to RIDW, the residuals are estimated by Equations (5) and (6), with the main difference that  $X_O$  corresponds to monthly gauge estimates and  $X_B$  represents the  $\text{CHIRPM}_m$  values computed at each gauge location. However, unlike RIDW, the residual field  $r_o$  is interpolated by ordinary kriging (Grimes *et al.* 1999) at each grid point and added back to  $\text{CHIRPM}_m$ .

To ensure the non-stationarity assumption, the residuals are converted to a logarithmic scale and back-transformed after the merging phase. In this study, the variogram adjustment is automatically performed based on Hiemstra *et al.* (2009). For more details on the implementation of ROK, refer to Goovaerts (2000).

#### 2.4.3 Monthly correction factor (Mcf)

Given that a higher spatial relationship is achieved at the monthly rather than at the daily time step (Ly *et al.* 2013),  $\text{PISCOp}_m$  is expected to present a higher performance

compared with the monthly aggregation of  $P\text{-PISCOp}_d$ . Therefore, based on Keller *et al.* (2015), a monthly correction factor (Mcf) was added after the creation of  $P\text{-PISCOp}_d$  and  $\text{PISCOp}_m$  with two purposes: to provide higher spatial consistency to daily predictions and to ensure that the monthly aggregation of the daily product matches the monthly product at each grid point. Thus, Mcf is calculated by:

$$\text{Mcf} = \begin{cases} \frac{\text{PISCOp}_m}{\sum_{i=1}^N P\text{-PISCOp}_{d(i)}} & \text{if } \text{Mcf} > 0 \\ 1 & \text{if } \sum_{i=1}^N P\text{-PISCOp}_{d(i)} = 0 \end{cases} \dots \quad (10)$$

where  $N$  is the number of days of the corresponding month. Finally,  $\text{PISCOp}_d$  is defined as:

$$\text{PISCOp}_d = P\text{-PISCOp}_d \times \text{Mcf} \quad (11)$$

### 2.5 Evaluation of PISCOp V.2.1

The process for evaluating the performance of PISCOp V2.1 was performed on the period 1981–2016 in two steps: Firstly, a pixel-to-point evaluation is carried out using an independent rainfall network (ID) which consists of 100 raingauges (Fig. 1(a)) not previously used for the development of PISCOp V2.1.

We selected all raingauges with >12 months of data between January 1981 and December 2016 that are located at a minimum distance of 20 km from the PISCOp raingauge network. Three continuous statistics are computed comparing the time series of PISCOp V2.1 and ID (Table 2). The Pearson correlation coefficient (CC) is used to evaluate the capability of PISCOp V2.1 to capture rainfall variability; the RMSE measures the average magnitude of the error; and the percent bias (PBIAS) indicates the degree to which each PISCOp V2.1 value is over- or under-estimated (Teng *et al.* 2014).

Additionally, following the criteria defined by Zambrano-Bigiarini *et al.* (2017), the three categorical statistics (Table 2) probability of detection (POD), false alarm rate (FAR) and threat score (TS) are used to determine PISCOp V2.1 rainfall detection capabilities within five precipitation intensity classes (Table 3). The POD and FAR indicate which fraction of the observed events are correctly detected and which fraction of the events reported by the GRDs did not occur. The TS is a general categorical statistic sensitive to hits and penalizes both missing and false alarms affected by the climatological frequency of the event. More information on the aforementioned indices can be found in Wilks (2006).

Secondly, a water balance evaluation using two simple runoff ratios (RR and RR<sub>f</sub>) is carried out in 19 Peruvian catchments using the following equations:

$$RR = \frac{Q}{P} \quad (12)$$

$$RR_f = \frac{Q}{(P - ET)} \quad (13)$$

where  $Q$ ,  $P$  and  $ET$  are the annual long-term average of the discharge, precipitation and real evapotranspiration,

**Table 2.** Continuous and categorical statistics.  $X$ : GRD estimate;  $Y$ : ID measurement;  $\bar{X}$ : GRD average;  $\bar{Y}$ : ID average;  $N$ : number of data pairs;  $A$ : number of hits;  $B$ : number of false alarms;  $C$ : number of misses; and  $D$ : number of correct negatives.

Statistic	Formula	Perfect score
<i>Continuous statistics</i>		
Correlation coefficient, CC	$CC = \frac{\sum(x-\bar{x})(y-\bar{y})}{\sqrt{\sum(x-\bar{x})^2 \sum(y-\bar{y})^2}}$	1
Root mean squared error, RMSE	$RMSE = \sqrt{\frac{1}{N} \sum (X - Y)^2}$	0
Percentage bias, PBIAS	$PBIAS = 100 \times \left[ \frac{\sum(x-y)}{\sum x} \right]$	0
<i>Categorical statistics</i>		
Probability of detection, POD	$POD = A / (A + C)$	1
False alarm ratio, FAR	$FAR = B / (A + B)$	0
Threat score, TS	$TS = A / (A + B + C)$	1

**Table 3.** Classification of rainfall events based on quantiles.

Quantile	Daily rain (mm/d)	Daily rainfall event
[0–0.1>] *	[0–1.5>]	No rain
[0.1–0.5>]	[1.5–5.3>]	Light rain
[0.5–0.9>]	[5.3–19.5>]	Moderate rain
[0.9–0.975 >]	[19.5–38.4>]	Heavy rain
0.975 >	38.4>	Violent rain

\*This rainfall class is considered as no rain.

respectively. Unlike the pixel-to-point approach, the runoff ratios (RR and RR<sub>f</sub>) allowed us to assess the long-term capacity of PISCOp V2.1 in more extensive areas. Due to the fact that the annual time step is a sufficiently large time period, we assume that the catchment storage is zero. Hence,  $Q$  and  $(P - ET)$  are expected to adopt similar values. The discharge gauge data ( $Q$ ) were obtained from the Environmental Research Observatory SO HYBAM ([www.ore-hybam.org](http://www.ore-hybam.org)) and SENAMHI (Table 4 and Fig. 1(b)). Due to data scarcity, the  $ET$  was computed based on a modification of the Budyko hypothesis (Fu's equation, Yao *et al.* 2016) and the gridded maximum and minimum temperature dataset generated for Peru by Vicente-Serrano *et al.* (2017). Four GRDs were used to estimate  $P$ : (a) PISCOp V2.1; (b) CHIRPM; (c) ORE-HYBAM (HOP, Guimberteau *et al.* 2012), which is only available for the Amazon and generated at 1° spatial resolution using ordinary kriging; and (d) the previous PISCOp version (V1.0), which is based on the merging between CHIRPS and raingauges applying kriging with external drift (Lavado *et al.* 2015). We used CHIRPM as a reference to explore possible improvements after the merging phase. We compared PISCO V2.1 and PISCOp V1.0 to examine the repercussions of changing CHIRPS by CHIRPM. The comparison to HOP serves to understand the role of the introduction of spatial predictors (CHIRPM). It is important to note that HOP, PISCOp V1.0 and PISCOp V2.1 present almost the same availability of raingauges within selected upstream catchments. Therefore, the influence of raingauge density can be handled as a common systematic variation for all GRDs used.

### 3 Results and discussion

#### 3.1 State and gap-infilling of the peruvian rainfall dataset

According to the three-step QC approach (Section 2.2.1), 3.51% of the total data (Table 5) had gross error and was deleted for the next steps. The most affected sub-region with data exclusion was the AW and the least affected was the PC. Hunziker *et al.* (2017b) indicated that a large fraction of gross errors are caused by observers during data recording, while Hunziker *et al.* (2017a) mentioned that due to these errors and a large amount of missing data, 40% of available raingauges are inappropriate for climate analyses. Following our approach, and considering that within the 1981–2016 period at least 10 years of continuous information must be available after applying QC, the number of stations had reduced from 945 to 441 (Fig. 1(a)). These raingauges (henceforth called PISCOp rainfall network) form the basis and constitute the most valuable source of information for the construction of the gridded dataset.

The density of the PISCOp rainfall network lies at around 282 per 10<sup>6</sup> km<sup>2</sup> for Peru (Table 5), with maximum density in AW and minimum in AL. These results suggest a remarkably heterogeneous distribution and very sparse conditions across the whole of Peru. Despite the data scarcity, the Peruvian rainfall network (Table 5) lies within the minimum requirements for hydrological analyses defined by the World

**Table 4.** Summary of *in situ* discharge gauge characteristics. ETP: potential evapotranspiration; ET: real evapotranspiration.

No.	Name	Code	Catchment area (km <sup>2</sup> × 10 <sup>-3</sup> )	Raingauge density (per 10 <sup>6</sup> km <sup>2</sup> )	Mean discharge (m <sup>3</sup> /s)	PISCOp V2.1 Precipitation (mm/year)	ETP	ET
1	Borja	BRJ	94.21	371.5	49.43	1730	973	799
2	Chazuta	CZT	69.57	445.6	30.76	2333	1043	936
3	Pucallpa	PCP	267.38	254.3	101.78	2047	996	881
4	Requena	RQN	359.26	203.2	123.34	2236	1351	1116
5	Ardilla	ARD	11.89	1093.2	1.49	916	1051	554
6	Puchaca	PCH	0.74	0	0.06	717	834	448
7	Condorcerro	CON	10.54	664.3	1.39	743	653	380
8	Yanapampa	YNP	4.27	703.3	0.41	470	678	199
9	Santo Domingo	SDG	1.89	1587.2	0.16	463	676	206
10	La Capilla	LCP	2.19	1370.8	0.19	541	695	242
11	S&T Imperial	SYT	5.96	1341.3	0.55	477	658	210
12	Conta	CNT	3.12	960.0	0.11	374	727	268
13	Letrayoc	LTY	3.57	1121.4s	0.26	502	669	304
14	Huatiapa	HTP	13.04	997.2	0.76	513	551	328
15	Chucarapi	CCP	13.51	592.2	0.32	300	604	235
16	La Tranca	LTC	2.01	993.1	0.02	123	665	93
17	Bella Union	BUN	4.30	465.5	0.12	204	698	122
18	Puente llave	ILV	8.12	369.2	0.32	304	523	173
19	Puente Ramis	RMS	15.09	596.2	0.72	597	549	422

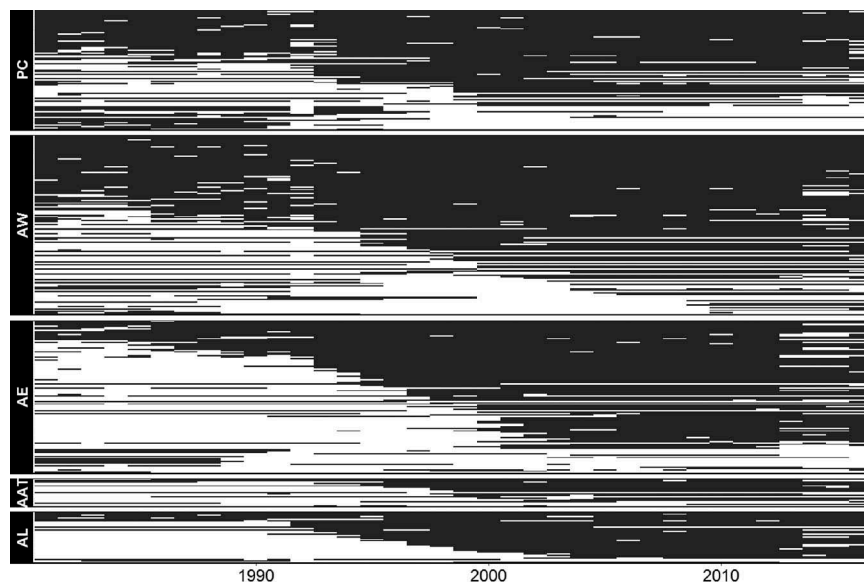
**Table 5.** Overview of the state and gap-infilling of the PISCOp rainfall network: BCC: percentage of gaps completed by bias-corrected CHIRPM (%);  $D_n$ : spatial average of KS statistic; and  $MK_{\text{bef-af}}$ : number of spurious trends after the gap-infilling procedure.

	Sub-region (total rain gauges: 441)					Total
	PC	AW	AE	AAT	AL	
<i>Monthly</i>						
Density (/10 <sup>6</sup> km <sup>2</sup> )	480	754	381	170	59	282
Gross error (%)	0.62	7.5	2.19	3.60	1.2	3.51
No data (%)	34.8	30.94	41.44	45.14	41.72	37.41
CUTOFF (%)	14.16	11.20	12.49	35.28	40.76	16.40
BCC (%)	20.64	19.74	28.95	10.05	0.96	21.01
$D_n$	0.07	0.05	0.04	0.03	0.02	0.05
<i>Daily</i>						
No data (%)	32.98	29.39	39.82	43.09	39.40	35.65
CUTOFF (%)	12.22	13.88	27.04	34.07	33.72	20.56
BCC (%)	20.76	15.51	12.78	9.02	5.68	15.09
$D_n$	0.03	0.03	0.05	0.07	0.03	0.03
$MK_{\text{bef-af}}$	4	1	7	3	3	18

Meteorological Organization (WMO 1994) and it is similar to the raingauge density presented in previous works related to

regional runoff simulation in adjacent regions of Peru (Guimberteau *et al.* 2012, Zulkafli *et al.* 2013, Getirana *et al.* 2014). Most of these raingauges are located in mountain recharge zones, which is an important condition for rainfall-runoff simulation in Pacific and Andean drainage catchments (Fig. 1). Nonetheless, the density of the PISCOp rainfall network is far below conventional climatological datasets worldwide (Hofstra *et al.* 2009, Yatagai *et al.* 2012, Newman *et al.* 2015, Lussana *et al.* 2018). Therefore, it is expected that regions with lower density introduce biases in the mean and variance of the gridded dataset.

The gaps in the raingauge series were identified as the main problem for the construction of a serially complete gauge dataset in Peru. In general, most raingauges belonging to the PISCOp rainfall network were installed after the year 2000, which explains the high percentage of missing data (34.74%) before this date (Fig. 3). For this reason, the amount of data available for the period 2001–2016 exceeds by 117%

**Figure 3.** Missing data for each sub-region. Note: the raingauges are ordered from lowest missing values (upper line) to highest missing values (lower line).



that for the period 1981–2000, with the most significant difference (204%) in the AL. The monthly gap-infilling approach based on neighbouring stations allowed us to infill 44% of total missing data, while the daily approach allowed 58% to be infilled (Table 5).

Considering the fact that the neighbouring information was not enough to create serially complete time series for all raingauges, bias-corrected CHIRPM was added. Similar to other studies (Chaney *et al.* 2014, Teegavarapu and Nayak 2017), we used the Mann-Kendall (MK) and Kolmogorov-Smirnov (KS) statistical tests to determine whether the performance of the gap-infilling procedure is appropriate.

Firstly, the KS nonparametric test, that does not use any distributional assumptions, was employed as a metric to estimate if the distribution before and after the gap-infilling procedure was identical. Considering a 5% significance level, 54 raingauges at the daily time step and 41 at the monthly time step were flagged for showing a poor match between the cumulative distribution functions ( $D_n > 0.1$ , see Supplementary material, Fig. S2). In addition, Table 5 indicates a spatial average of  $D_n$  below 0.07 for all the sub-regions.

Next, to identify the possible formation of spurious trends, the MK test was performed on annual time series from the period 1981–2016. At a 5% significance level, 18 raingauges (see Supplementary material, Fig. S2) were identified with positive trends ( $\tau > 0.1$ ).

Both results suggest that the gap-infilling procedure adopted in this study is acceptable, showing an unclear spatial pattern in the results (Supplementary material, Fig. S2). Nonetheless, note that ~14% of the raingauges were flagged by at least one of the tests. Therefore, it is expected that inhomogeneities are present in the serially complete gauge dataset. For an individual inspection of the gap-infilling procedure, see <http://piscoprec.github.io/gauge>.

### 3.2 Spatial description of PISCOp

The rainfall pattern for January 1998 (Fig. 4) and day 25 of this month (Fig. 5) were used to perform a visual check of PISCOp products (PISCOp<sub>m</sub> and PISCOp<sub>d</sub>, Fig. 2). This date was selected as an atypical and violent rainfall event (Table 3), caused by the ENSO phenomenon, was experienced on this day in the north of Peru.

The output analysis for January 1998 was performed considering as a reference the rainfall measured in this month by the PISCOp rainfall network (Fig. 4(a)). Thus, CHIRPM (Fig. 4(b)) only shows an acceptable representation of the spatial structure of the rainfall field within the AW, while for the AE, AAT and AL, a remarkable underestimation is evident with increasing rainfall rates. Underestimation of TIR-based GRDs, such as CHIRPM, for high rainfall values is a well-known condition (Kidd and Huffman 2011). In contrast, the PC shows unrealistically high rain values for the entire study period (1981–2016). This pattern is a consequence of the CHP<sub>clim</sub> used as a spatial predictor; CHP<sub>clim</sub> reasonably depicts the spatial structure in the PC. Nonetheless, the lack of raingauges for calibration produces severe overestimation of rainfall amounts (Fig. S1). Regarding the CHIRPM<sub>m</sub> product (Fig. 4(c)), in general, it improved the

rainfall characterization in most of the sub-regions in comparison to CHIRPM. This improvement is explained by the use of PISCO<sub>clim</sub> instead of CHP<sub>clim</sub> in the CHIRPM<sub>m</sub> construction. However, it is still unable to detect the convective storms caused by the ENSO in the northern PC.

In contrast to CHIRPM and CHIRPM<sub>m</sub>, the PISCOp<sub>m</sub> product (Fig. 4(d)) underlies different rainfall intensities and spatial structure of the entire study area. These changes are the result of the interaction of: (a) spatial autocorrelation among residuals (measured through the semivariogram), (b) the distribution of the PISCOp rainfall network, and (c) the magnitude and sign of the residuals. For the analysed month, negative residuals and a considerable number of raingauges led to a rainfall increase in the AE and AW, as well as to a better representation of the spatial pattern caused by ENSO in the northern PC. Likewise, the Peruvian Amazon areas (AAT and AL) also show negative residuals, although the reduced number of raingauges led to a high negative local average. Therefore, a scenario with high rainfall amounts is expected, especially when the de-correlation distance is overcome.

Even though the use of geostatistical interpolation methods allows the spatial coherence to be maximized, it must be taken into account that the predicted values in PISCOp<sub>m</sub> may differ from the raingauge values particularly related to the formation of large residuals. This behaviour has already been extensively described in Tozer *et al.* (2012) and further studies (Ensor and Robeson 2008, Hofstra *et al.* 2009, Erdin *et al.* 2012). Therefore, special care must be taken when using PISCOp V2.1 for analysing extreme events, such as those related to ENSO.

For the blending process at a daily time step, several products (CHIRPM<sub>d</sub>, P-PISCOp<sub>d</sub> and Mcf), were created before generating the final dataset PISCOp<sub>d</sub>. In previous studies, it has been demonstrated that in data-scarce regions the areal rainfall estimates are better represented in blended than in the only gauge-based GRDs (Buytaert *et al.* 2006, Schuurmans *et al.* 2007, Nerini *et al.* 2015). Hence, P-PISCOp (Fig. 5(c)) was produced by merging the serially complete PISCOp<sub>d</sub> rainfall network (Fig. 5(a)) with CHIRPM<sub>d</sub> (Fig. 5(b)). Unlike CHIRPM<sub>d</sub>, P-PISCOp allowed an admissible characterization of convective storms that occurred at the northern PC and improved the rainfall scenario in the AW. Nonetheless, a marked underestimation concerning CHIRPM<sub>d</sub> was found for the rainy pixels located at the centre of the AAT and AL. The explanation of this change is similar to the previous month analysed, with the difference that at daily time step the predictor (CHIRPM<sub>d</sub>) represents the spatial variance being worse, causing higher instability in the residuals. Due to the absence of raingauges, the residuals of the western sub-regions (PC, AW and AE) are continuously and omnidirectionally transferred to the eastern sub-regions (AAT and AL) by IDW. The efficiency of this process directly depends on the residuals variance and intermittent rainfall regime (Chappell *et al.* 2012). A scenario with low variance and intermittency should improve the systematic bias; otherwise, this transfer would result in inaccurate precipitation values (Fig. 5(c)). Finally, PISCOp<sub>d</sub> (Fig. 5(d)),

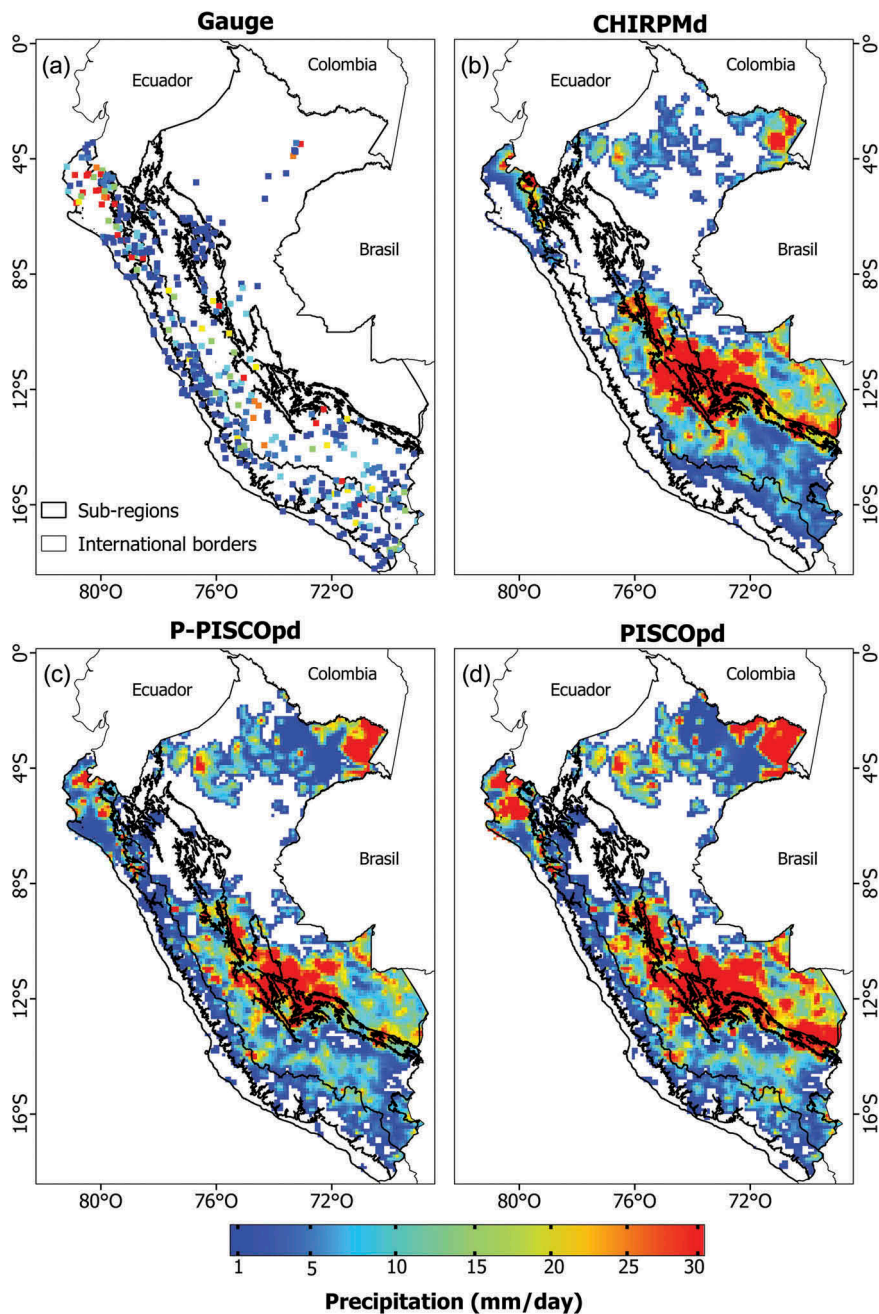


Figure 4. Spatial distribution of rainfall for January 1998: (a) rainfall network, (b) CHIRPM, (c) CHIRPM<sub>m</sub> and (d) PISCOP<sub>m</sub>.

unlike P-PISCOP<sub>d</sub>, decreases the bull's-eye effect formation around the gauge observations relying on the spatial structure of PISCOP<sub>m</sub>. Besides, a clear precipitation increase can be observed for the AL and AAT due to the formation of Mcf values > 1 in these sub-regions.

### 3.3 Performance of PISCOP V.2.1

As may be seen in Fig. 6, the sub-regions PC and AW show the most significant improvements for PISCOP V.2.1 compared to CHIRPM, although there is a slight increment in the spread of their scores. In these sub-regions, P-PISCOP<sub>d</sub> and PISCOP<sub>d</sub> (PISCOP<sub>m</sub>) increase the accuracy of the CC to 213% and 210% (14%) compared to CHIRPM<sub>d</sub> (CHIRPM<sub>m</sub>). The RMSE values show consistent reduction in random error and

the systematic PBIAS is close to 0. For the AE and AAT, the performance of PISCOP V.2.1 continues to indicate a substantial increase (reduction) of the CC (RMSE) score with respect to CHIRPM, although these values are worse in comparison to the PC and AW. This can be explained by a lower density of raingauges and that TIR-based retrieval algorithms imply a poorer performance under high influence of topographic complexity (Thouret *et al.* 2013, Mantas *et al.* 2015, Derin *et al.* 2016). At the monthly time step, PISCOP<sub>m</sub> provides higher accuracy in capturing the influence of the ITCZ migration through the tropical Andes, despite a remarkable underestimation of the precipitation gradients for the eastern Andean slopes. In contrast, at the daily time step, P-PISCOP<sub>d</sub> and PISCOP<sub>d</sub> showed a poor performance that did not lead to any improvement compared to

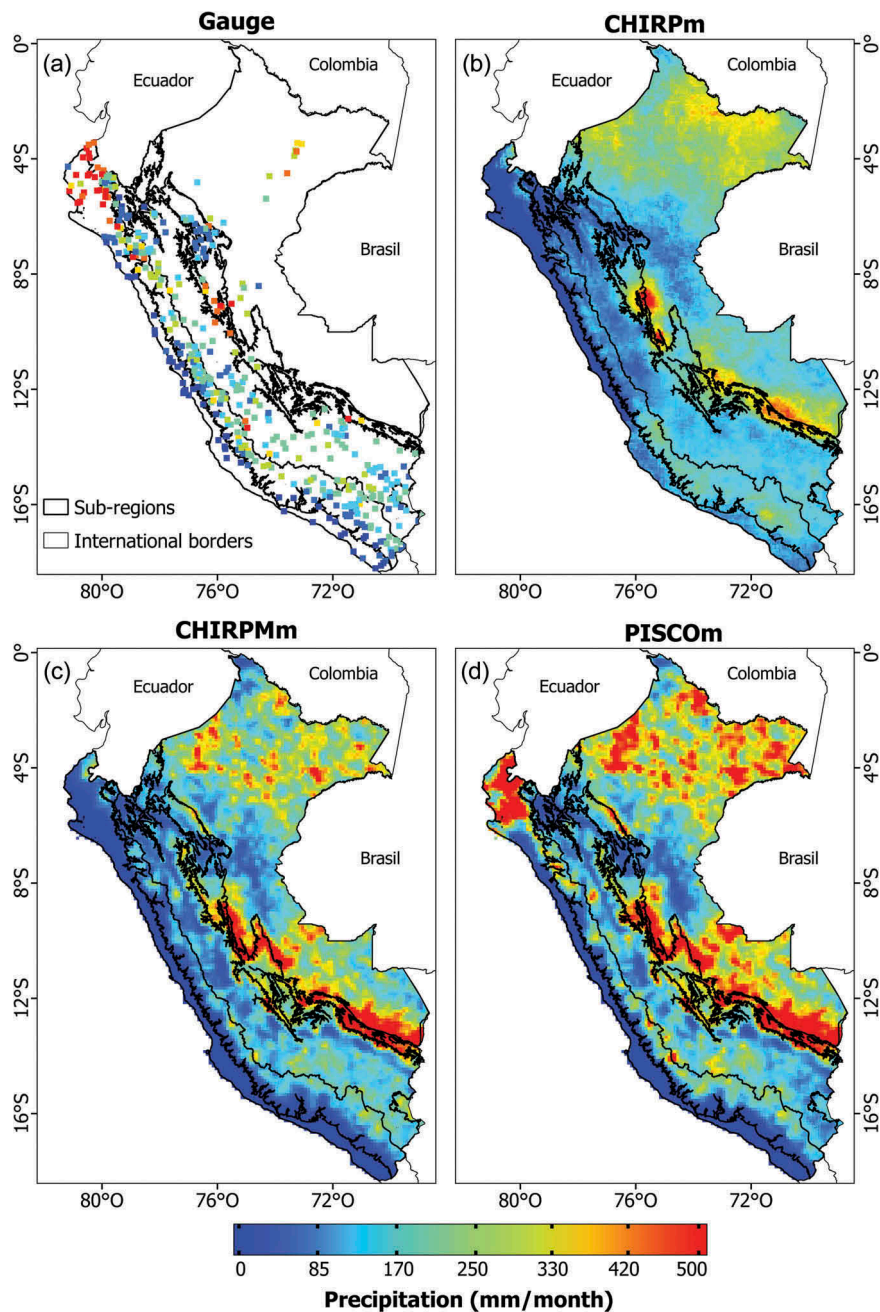


**Figure 5.** Spatial distribution of rainfall for 25 January 1998: (a) the rainfall network, (b) CHIRPm, (c) P-ISCOm and (d) ISCOm. Only values >1 mm are plotted.

CHIRPm<sub>d</sub>. Finally, the AL presented the largest RMSE score and lowest CC of our study area. Even at the monthly time step, PISCOm presented a lower performance than CHIRPm<sub>m</sub>. Similar results have recently been reported for the Ecuadorian Amazon by Ulloa *et al.* (2017), who state that the reduced number of rain gauges used for the merging phase generates spatial inconsistencies for the entire analysis period.

According to the categorical indices applied in this study, both P-ISCO<sub>d</sub> and ISCO<sub>d</sub> presented similar scores that were higher than CHIRPm<sub>d</sub> in the entire study area (Fig. 7). In general, the detection capacity of the three products weakens as the precipitation intensity category increases (Table 3), regardless of the geographical position. Comparing the categories “no rain” and “violent rain”, the POD score decreased and FAR increased drastically by 452% and 245%,

respectively. The TS showed that the daily products, CHIRPm<sub>d</sub>, PISCO<sub>d</sub> and P-ISCO<sub>d</sub>, were not able to correctly capture the fraction of rainfall events for all sub-regions. These results show that these daily PISCO products are most likely not sufficiently accurate for capturing heavy rainfall events. Hence, the use of PISCO products to describe the intensity of extreme precipitation events is not recommended if no high-density rainfall network exists nearby.

Figure 8 illustrates the water balance evaluation of PISCO V2.1, CHIRPm and two other GRDs (PISCO V1.0 and HOP) using runoff ratios (RR and RR<sub>f</sub>). The widest spread in RR and RR<sub>f</sub> scores was observed within the Amazon basin, indicating that PISCO V2.1 reaches a similar score to HOP, while it has an underestimation of 15% for CHIRPm and an



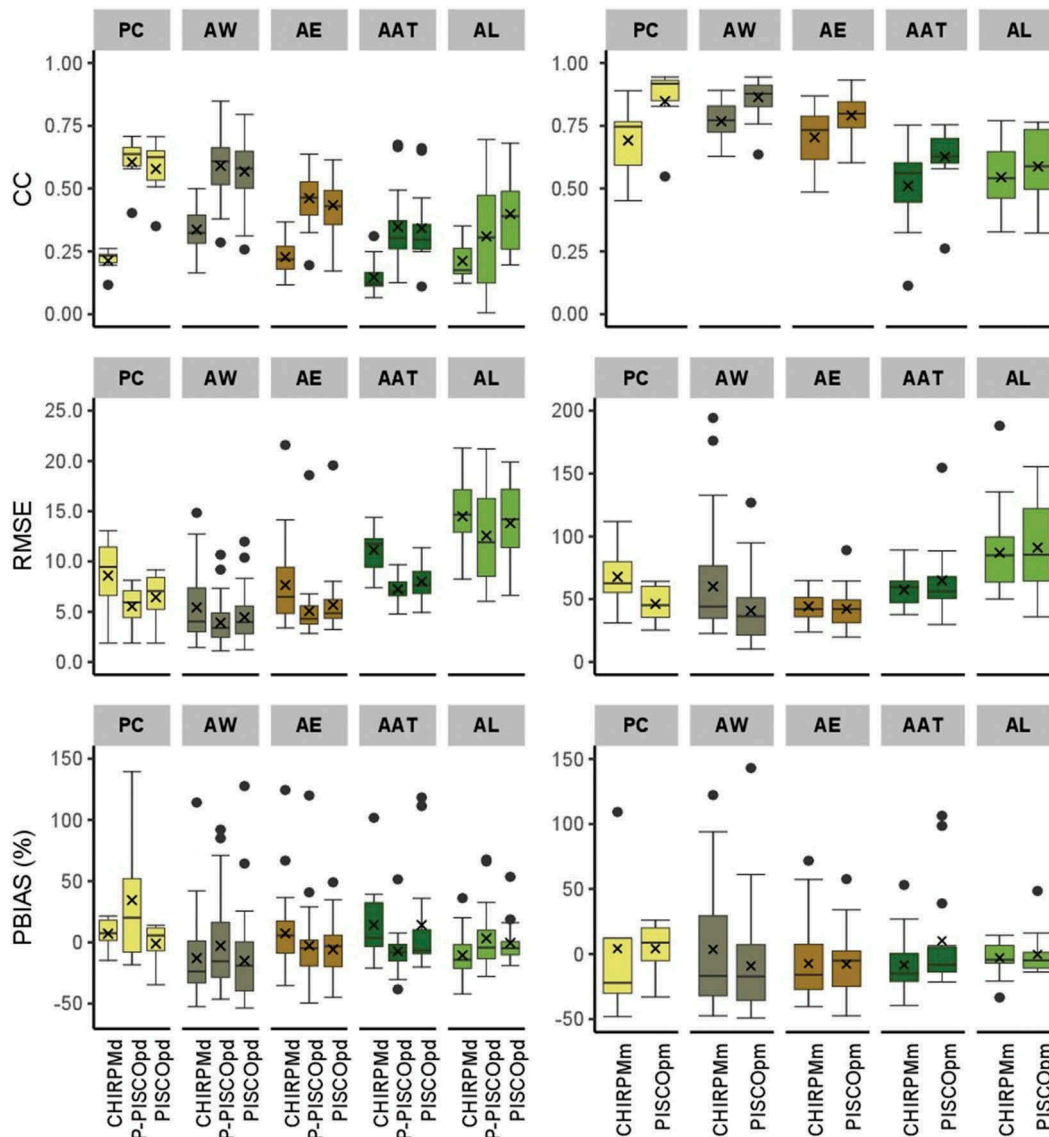


Figure 6. Boxplots of continuous statistics (CC, RMSE and PBIAS) between the daily and monthly products of PISCOP V.2.1 and ID. The cross represents the spatial average.

overestimation of 28% for PISCOP V1.0. For the Amazon, RR estimates are typically below 0.8 (Costa and Foley 1997, Rudorff *et al.* 2014, Gusev *et al.* 2017), while the average RR values for PISCOP V.2.1, CHIRPM, PISCOP V1.0 and HOP are around 0.89, 0.75, 1.05 and 0.88, respectively. Similar results were found for  $RR_f$ , with PISCOP V2.1, CHIRPM and HOP having values close to 1 ( $-0.2 < RR_f < 0.2$ ). Although these high runoff ratios could be explained by excessive groundwater contribution (Zubieta *et al.* 2015), a rainfall underestimation scenario is a more likely explanation, especially when considering the independent validation results which indicate the PBIAS trend to be negative (Fig. 6). The  $RR_f$  within the Amazon shows that CHIRPM achieves the best agreement with discharge values. Additionally, the climate correction based on PISCOP<sub>clim</sub> (used in CHIRPM and PISCOP V2.1) led to a better performance than CHP<sub>clim</sub> (used in PISCOP V1.0) in order to eliminate the underestimation of rainfall, particularly on the eastern slopes of the Andes. For catchments covering the Andes or Pacific, CHIRPM, PISCOP V1.0 and PISCOP V2.1 present very slight

differences in their RR and  $RR_f$  scores, with values mostly below 1. Unlike the Amazon, in the Andes-Pacific the change from CHP<sub>clim</sub> to PISCOP<sub>clim</sub> did not affect the areal rainfall estimations, possibly due to a better distribution and higher density of the rainfall network. The  $RR_f$  values of CHIRPM, PISCOP V2.1 and PISCOP V1.0 exhibited a systematic overestimation mainly for catchments  $>10\,000\text{ km}^2$  (Fig. 8). This uncertainty could be related to streamflow alteration caused by anthropogenic factors or low ET estimates. However, it is difficult to predict and beyond the scope of this investigation.

### 3.4 Impacts and detection of inhomogeneities

All inputs used for the development of PISCOP V2.1 are not thoroughly homogenized. The Peruvian long-term gauge dataset is affected by a plethora of non-climatic factors, such as changes of instruments or bad observer practices (Peterson *et al.* 1998, New *et al.* 2000, Brönnimann 2015). Also, inconsistencies are also present in the CHIRP algorithm. For instance, they arise when infilling missing CHIRP values



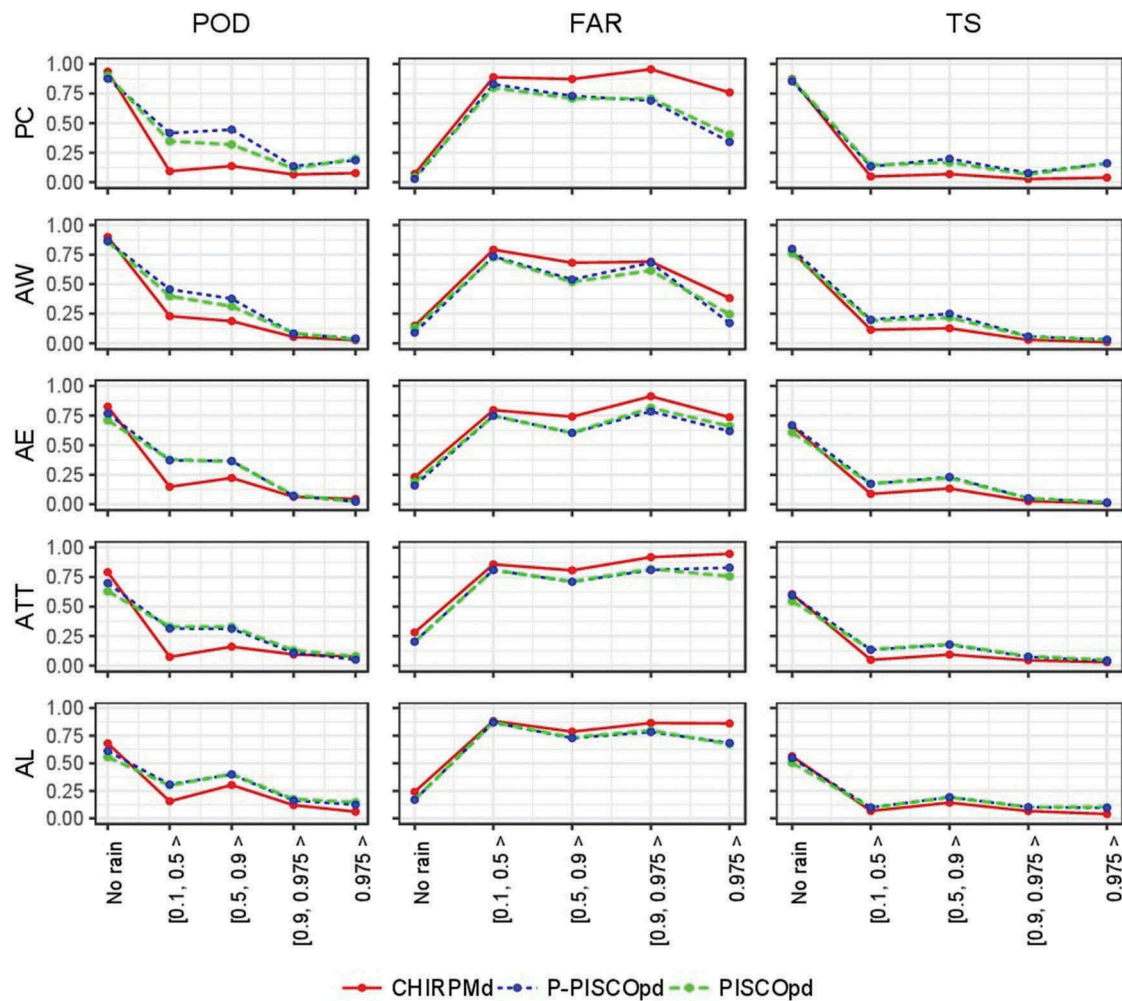


Figure 7. Categorical validation statistics of PISCOpd products in five quantile classes of rainfall intensity for the five sub-regions (see Table 3).

with the Coupled Forecast System version 2 (Saha *et al.* 2014), or in the overlap between the TIR archives: Globally Gridded Satellite (GriSat) and NOAA Climate Prediction Center (CPC; Funk *et al.* 2015a). In order to detect a spatial pattern in these inhomogeneities, we applied the Pettitt test, with a significance level of 5%, for annual time series of each PISCOp V2.1 grid cell, and for the water balance estimation, we used CHIRPM, PISCOp V1.0, and HOP as a reference. Figure 9(a) shows the years when a breakpoint was detected. In general, the three GRDs indicate wide variability in their breakpoint years and spatial extent. CHIRPM obtained the smaller inhomogeneity area within the Amazon basin (8.1%), followed by PISCOp V.2.1 (8.2%), HOP (34%) and PISCOp V1.0 (89%). The breakpoint year observed for CHIRPM is associated with the transition from GriSat to CPC, whereas the breakpoint for PISCOp V1.0 notably coincides with the changes in the density of the PISCOp rainfall network (Fig. 3). Regarding PISCOp V2.1 and HOP, the inhomogeneity area drastically decreased due to the data gap infilling performed at each station and a further balancing-out during the geostatistical interpolation. Although breakpoints in rainfall time series can naturally occur, no evidence was found for any of the 56 raingauges with more than 95% of complete time series (Fig. 1(a)).

Based on the breakpoints detected for each cell, a sensitive area (Fig. 9(a)) was defined to analyse the plausibility of the time series in more detail. As shown in Fig. 8(b), the intensities, breakpoint year at 5% significance level (red dotted line) and seasonality of the three GRDs at the monthly time step vary considerably despite using similar inputs. The inhomogeneities in the GRDs imply severe impacts for the analysis of the seasonal (not shown here) and annual trend (Fig. 9(c)). For the assessment of these impacts, Sen's slope estimator at the 95% confidence level was used. For the 1981–2016 period, PISCOp V2.1, PISCOp V1.0 and HOP revealed a significant positive trend that exceeded 55%, 81% and 72%, respectively, in the slope of CHIRPM. Artificial trends (Hofstra *et al.* 2010, Nicolas and Bromwich 2011, Tozer *et al.* 2012, Kingdom 2014) are principally spread across the entire Peruvian Amazon, especially where data scarcity prevails and there is a high amount of gaps.

#### 4 Summary and conclusions

In this paper, we presented the development of PISCOp V2.1, a new daily and monthly long-term GRD for the period 1981 to the present. This gridded product was generated based on the integration of serially complete gauge datasets, CHIRP

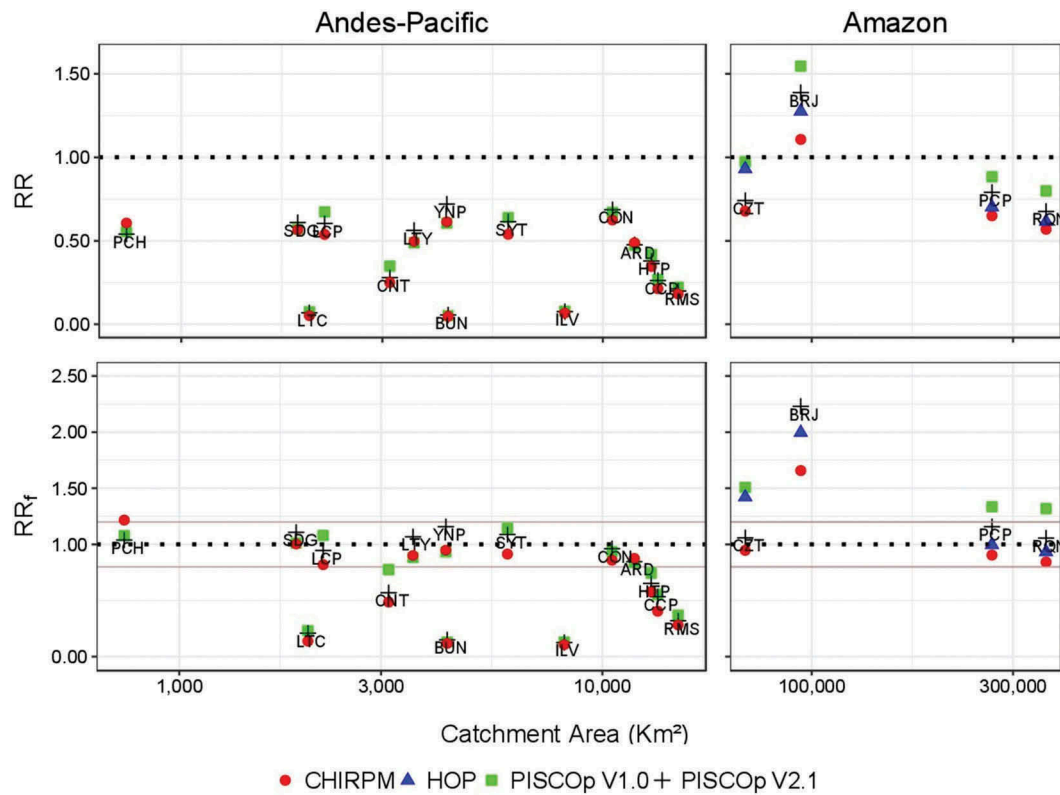


**Figure 8.** Runoff ratios (RR and RR<sub>f</sub>) between different GRDs (PISCOp V2.1, CHIRPM, PISCOp V1.0 and HOP) and discharge observations for catchments draining within the Andes-Pacific (left) and Amazon (right).

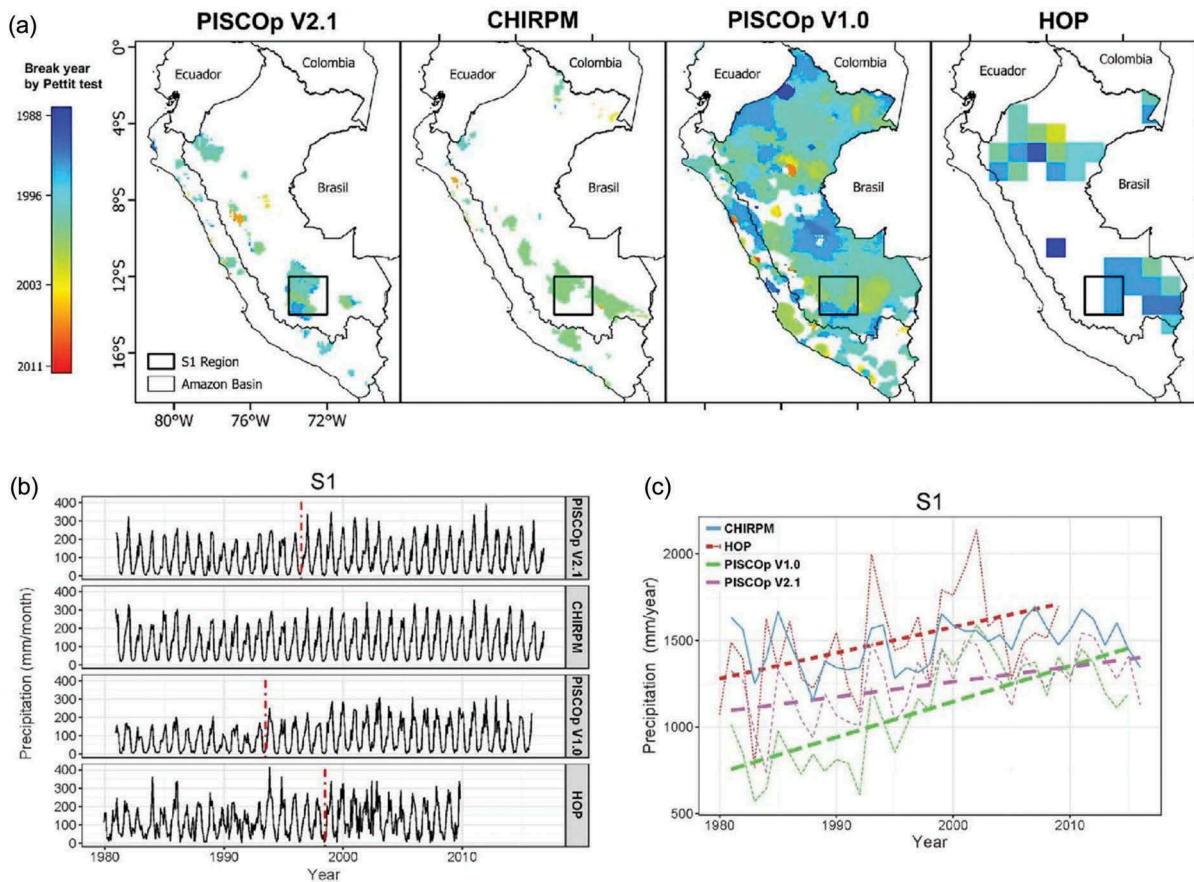


**Figure 9.** (a) Spatial distribution of break year (calculated by Pettit test) in annual time series of PISCOp V2.1, CHIRPM, PISCOp V1.0 and HOP. Only values at 95% significance level ( $p < 0.05$ ) are plotted. (b) Areal monthly precipitation for the S1 region. The breaks at 95% significance level are plotted on the vertical dotted (red) line. (c) Evolution of the average annual rainfall in the S1 region. Only trend lines with a significant level of 95% are plotted.

data, radar-based climatologies and geostatistical and deterministic interpolation methods. The quality of PISCOP V2.1 was assessed within six hydro-meteorological sub-regions with an independent raingauge network. Additionally, the runoff ratio estimation within 19 catchments allowed us to evaluate the performance of PISCOP V2.1 in more extensive areas.

For the first time, PISCOP V2.1 comprehensively presents the state of the Peruvian raingauge dataset for the period 1981–2016. It has been identified that the gaps in rainfall time series represent the most determining problem for the construction of a temporally consistent GRDs. This study shows that the combinations between both CUTOFF and Qm are a conservative and efficient method for successful data gap-infilling, especially for large data gaps that prevail at the beginning of the PISCOP V2.1 period. However, this method strongly depends on the predictor and the proximity of raingauges. Hence, it is expected that application of our approach to areas with low station density and poor performance of CHIRPM might lead to unsatisfactory results.

The independent and water balance evaluations confirm that PISCOP V2.1 is the most suitable product for representing areal rainfall estimates, except for the Amazon lowland where CHIRPM had improved outcomes. Additionally, we note that the climatological correction based on PISCOP<sub>clim</sub> significantly improved the results compared to CHP<sub>clim</sub>. At the daily time step, PISCOP<sub>d</sub> did not capture the convective storm intensity, regardless of the geographical position. Although it seems highly attractive to use gridded data with full spatial and temporal coverage, such as PISCOP V2.1, all inhomogeneities inherent to this merged product and presented in this study must be entirely taken into account. Therefore, as for other blended GRD products (Yanto *et al.* 2017, Beck *et al.* 2017a), we recommend users to take special care when using PISCOP V2.1 for the analysis of trends, extreme events or other applications related to e.g. climate change.

New versions of PISCOP have been planned and it is expected to make use of new existing information sources, such as IMERG (Huffman *et al.* 2015), cross-border raingauges, as well as to improve the data gap-infilling of rainfall time series.

## 5 Data access

The PISCOP V2.1 product, source code and additional information are freely available to users in NetCDF (1981–2016) and GeoTIFF (1981–present) format at the following website: <https://piscoprec.github.io/>.

## Acknowledgements

We thank SENAMHI and CLIMANDES for supporting this research and acknowledge hundreds of hydrometeorological observers around Peru for their work, which has made this study possible. The authors would like to thank Stephanie Gleixner, Fred F. Hattermann, Fabian Drenkhan and the anonymous reviewers for their valuable comments.

## Disclosure statement

No potential conflict of interest was reported by the authors.

## References

- Adhikary, S.K., 2017. Cokriging for enhanced spatial interpolation of rainfall in two Australian catchments. *Hydrological Processes*, 31 (March), 2143–2161. doi:10.1002/hyp.11163
- Antico, P.L., 2009. Relationships between autumn precipitation anomalies in Southeastern South America and El Niño event classification. *International Journal of Climatology*, 29 (July 2008), 719–727. doi:10.1002/joc
- Babak, O. and Deutsch, C.V., 2009. Statistical approach to inverse distance interpolation. *Stochastic Environmental Research and Risk Assessment*, 23 (5), 543–553. doi:10.1007/s00477-008-0226-6
- Baik, J., *et al.*, 2015. Geospatial blending to improve spatial mapping of precipitation with high spatial resolution by merging satellite- and ground based data. *Hydrological Processes*, 30 (16), 2789–2803. doi:10.1002/hpy.10786
- Beck, H.E., *et al.*, 2017a. MSWEP: 3-hourly 0.25° global gridded precipitation (1979–2015) by merging gauge, satellite, and reanalysis data. *Hydrology and Earth System Sciences*, 21 (1), 589–615. doi:10.5194/hess-21-589-2017
- Beck, H.E., *et al.*, 2017b. Global-scale evaluation of 23 precipitation datasets using gauge observations and hydrological modeling. *Hydrology and Earth System Sciences Discussions*, 21 (August), 1–23. doi:10.5194/hess-2017-508
- Beck, H.E., *et al.*, 2019. MSWEP V2 global 3-hourly 0.1° precipitation. *Bulletin of the American Meteorological Society*. 100 (March), 473–500. doi:10.1175/BAMS-D-17-0138.1
- Beguiría, S., *et al.*, 2015. Bias in the variance of gridded data sets leads to misleading conclusions about changes in climate variability bias in the variance of gridded data sets leads to misleading. *International Journal of Climatology*, 36 (December), 3413–3422. doi:10.1002/joc.4561
- Bi, S., *et al.*, 2017. A double-smoothing algorithm for integrating satellite precipitation products in areas with sparsely distributed in situ networks. *Isprs International Journal of Geo-Information*, 6 (1), 28. doi:10.3390/ijgi6010028
- Boers, N., *et al.*, 2013. Complex networks identify spatial patterns of extreme rainfall events of the South American monsoon system. *Geophysical Research Letters*, 40, 1–7. doi:10.1002/grl.50681
- Bookhagen, B. and Strecker, M.R., 2008. Orographic barriers, high-resolution TRMM rainfall, and relief variations along the Eastern Andes. *Geophysical Research Letters*, 35 (6), 1–6. doi:10.1029/2007GL032011
- Brönnimann, S., 2015. *Climatic changes since 1700*. Cham, Switzerland: Springer International Publishing. doi:10.1007/978-3-319-19042-6\_4
- Buytaert, W., *et al.*, 2006. Spatial and temporal rainfall variability in mountainous areas: a case study from the South Ecuadorian Andes. *Journal of Hydrology*, 329 (3–4), 413–421. doi:10.1016/j.jhydrol.2006.02.031
- Camposano, L., *et al.*, 2016. Rainfall and cloud dynamics in the Andes: a Southern Ecuador case study. *Advances in Meteorology*, 2016, 1–15. doi:10.1155/2016/3192765
- Carvalho, L.M.V., *et al.*, 2011. Moisture transport and intraseasonal variability in the South America monsoon system. *Climatic dynamics*, 36 (9–10), 1865–1880. doi:10.1007/s00382-010-0806-2
- Chaney, N.W., *et al.*, 2014. Development of a high-resolution gridded daily meteorological dataset over Sub-Saharan Africa: spatial analysis of trends in climate extremes. *Journal of Climate*, 27 (15), 5815–5835. doi:10.1175/JCLI-D-13-00423.1
- Chappell, A., Renzullo, L., and Haylock, M., 2012. Spatial uncertainty to determine reliable daily precipitation maps. *Journal of Geophysical Research: Atmospheres*, 117 (September), 1–14. doi:10.1029/2012JD017718
- Chavez, S.P. and Takahashi, K., 2017. Orographic rainfall hot spots in the Andes-Amazon transition according to the TRMM precipitation radar and in situ data. *Journal of Geophysical Research: Atmospheres*. doi:10.1002/2016JD026282
- Chen, F.W. and Liu, C.W., 2012. Estimation of the spatial rainfall distribution using inverse distance weighting (IDW) in the middle of Taiwan. *Paddy and Water Environment*, 10 (3), 209–222. doi:10.1007/s10333-012-0319-1



- Costa, M.H. and Foley, J.A., 1997. Water balance of the Amazon Basin: dependence on vegetation cover and canopy conductance. *Journal of Geophysical Research*, 102 (D20), 23973. doi:10.1029/97JD01865
- Derin, Y., et al., 2016. Multiregional satellite precipitation products evaluation over complex terrain. *Journal of Hydrometeorology*, 17 (6), 1817–1836. doi:10.1175/JHM-D-15-0197.1
- Dinku, T., et al., 2014. Combined use of satellite estimates and rain gauge observations to generate high-quality historical rainfall time series over Ethiopia. *International Journal of Climatology*, 34 (7), 2489–2504. doi:10.1002/joc.3855
- Ensor, L.A. and Robeson, S.M., 2008. Statistical characteristics of daily precipitation: comparisons of gridded and point datasets. *Journal of Applied Meteorology and Climatology*, 47 (9), 2468–2476. doi:10.1175/2008JAMC1757.1
- Erdin, R., Frei, C., and Künsch, H.R., 2012. Data transformation and uncertainty in geostatistical combination of radar and rain gauges. *Journal of Hydrometeorology*, 13 (4), 1332–1346. doi:10.1175/JHM-D-11-096.1
- Feng, L., et al., 2014. CUTOFF: a spatio-temporal imputation method. *Journal of Hydrology*, 519, 3591–3605. doi:10.1016/j.jhydrol.2014.11.012
- Funk, C., et al., 2015a. The climate hazards infrared precipitation with stations — a new environmental record for monitoring extremes. *Scientific data*, 2, 1–21. doi:10.1038/sdata.2015.66
- Funk, C., et al., 2015b. A global satellite-assisted precipitation climatology. *Earth System Science Data*, 7 (2), 275–287. doi:10.5194/essd-7-275-2015
- Garreaud, R., 1999. Multiscale analysis of the summertime precipitation over the Central Andes. *Monthly Weather Review*, 127 (5), 901–921. doi:10.1175/1520-0493(1999)127<0901:MAOTSP>2.0.CO;2
- Garreaud, R.D., et al., 2009. Present-day South American climate. *Palaogeography, Palaeoclimatology, Palaeoecology*, 281 (3–4), 180–195. doi:10.1016/j.palaeo.2007.10.032
- Getirana, A.C.V., et al., 2014. Water balance in the Amazon Basin from a land surface model ensemble. *Journal of Hydrometeorology*, 15 (6), 2586–2614. doi:10.1175/JHM-D-14-0068.1
- Goovaerts, P., 2000. Geostatistical approaches for incorporating elevation into the spatial interpolation of rainfall. *Journal of Hydrology*, 228 (1–2), 113–129. doi:10.1016/S0022-1694(00)00144-X
- Grimes, D.I.F., Pardo-Igúzquiza, E., and Bonifacio, R., 1999. Optimal areal rainfall estimation using rain gauges and satellite data. *Journal of Hydrology*, 222 (1–4), 93–108. doi:10.1016/S0022-1694(99)00092-X
- Gudmundsson, L., et al., 2012. Technical note: downscaling RCM precipitation to the station scale using statistical transformations. A comparison of methods. *Hydrology and Earth System Sciences*, 16 (9), 3383–3390. doi:10.5194/hess-16-3383-2012
- Guimberteau, M., et al., 2012. Discharge simulation in the Sub-Basins of the Amazon using ORCHIDEE forced by new datasets. *Hydrology and Earth System Sciences*, 16 (3), 911–935. doi:10.5194/hess-16-911-2012
- Gusev, Y.M., et al., 2017. Modelling river runoff and estimating its weather-related uncertainty for 11 large-scale rivers located in different regions of the globe. *Hydrology Research*, 2013, nh2017015. doi:10.2166/nh.2017.015
- Hamada, A., and Takayabu, Y.N., 2014. A removal filter for suspicious extreme rainfall profiles in TRMM PR 2A25 version-7 data. *Journal of Applied Meteorology and Climatology*, 53, 1252–1271. doi:10.1175/JAMC-D-13-099.1
- Hiemstra, P.H., Pebesma, E.J., and Twenho, C.J.W., 2009. Computers and geosciences real-time automatic interpolation of ambient gamma dose rates from the Dutch radioactivity monitoring network. *Computers & Geosciences*, 35, 1711–1721. doi:10.1016/j.cageo.2008.10.011
- Hofstra, N., et al., 2009. Testing E-OBS European high-resolution gridded data set of daily precipitation and surface temperature. *Journal of Geophysical Research: Atmospheres*, 114 (November). doi:10.1029/2009JD011799
- Hofstra, N., New, M., and McSweeney, C., 2010. The influence of interpolation and station network density on the distributions and trends of climate variables in gridded daily data. *Climate Dynamics*, 35 (5), 841–858. doi:10.1007/s00382-009-0698-1
- Houze, R.A., et al., 2015. The variable nature of convection in the tropics and subtropics: a legacy of 16 years of the tropical rainfall measuring mission satellite. *Reviews of Geophysics*, 53, 994–1021. doi:10.1002/2015RG000488.Received
- Huffman, G.J., et al., 2007. The TRMM multisatellite precipitation analysis (TMPA): quasi-global, multiyear, combined-sensor precipitation estimates at fine scales. *Journal of Hydrometeorology*, 8 (1), 38–55. doi:10.1175/JHM560.1
- Huffman, G.J., Bolvin, D.T., and Nelkin, E.J., 2015. Integrated multi-satellite retrievals for GPM (IMERG) technical documentation. *NASA/GSFC Code*, 612 (February), 47. doi:10.1136/openhrt-2016-000469
- Hunziker, S., et al., 2017a. Effects of undetected data quality issues on climatological analyses. *Climate of the Past Discussions*. 14 (May), 1–31. doi:10.5194/cp-2017-64
- Hunziker, S., et al., 2017b. Identifying, attributing, and overcoming common data quality issues of manned station observations. *International Journal of Climatology*, 37, 4131–4145. doi:10.1002/joc.5037
- Iguchi, T., et al., 2000. Rain-profiling algorithm for the TRMM precipitation radar. *Journal of Applied Meteorology*, 39 (12), 2038–2052. doi:10.1175/1520-0450(2001)040<2038:RPAFTT>2.0.CO;2
- Isotta, F.A., et al., 2014. The climate of daily precipitation in the Alps: development and analysis of a high-resolution grid dataset from pan-alpine rain-gauge data. *International Journal of Climatology*, 34 (5), 1657–1675. doi:10.1002/joc.3794
- Javier, F., et al., 2016. Intercomparison of improved satellite rainfall estimation with CHIRPS gridded product and rain gauge data over Venezuela. *Atmósfera*, 29 (4), 323–342. doi:10.20937/ATM.2016.29.04.04
- Joyce, R.J., et al., 2004. CMORPH: a method that produces global precipitation estimates from passive microwave and infrared data at high spatial and temporal resolution. *Journal of Hydrometeorology*, 5, 487–503. doi:10.1175/1525-7541(2004)005<0487:CAMTPG>2.0.CO;2
- Keller, V.D.J., et al., 2015. CEH-GEAR: 1 Km resolution daily and monthly areal rainfall estimates for the UK for hydrological and other applications. *Earth System Science Data*, 7 (1), 143–155. doi:10.5194/essd-7-143-2015
- Kidd, C. and Huffman, G., 2011. Review global precipitation measurement. *Meteorological Applications*, 353, 334–353. doi:10.1002/met.284
- Kingdom, U., 2014. Advances in the stochastic modeling of satellite-derived rainfall estimates using a sparse calibration dataset. *Journal of Hydrometeorology*, 15 (5), 1810–1831. doi:10.1175/JHM-D-13-0145.1
- Lavado Casimiro, W.S., et al., 2012. Basin-scale analysis of rainfall and runoff in Peru (1969–2004): Pacific, Titicaca and Amazonas Drainages. *Hydrological Sciences Journal*, 57 (4), 625–642. doi:10.1080/02626667.2012.672985
- Lavado, W., et al., 2015. PISCO: peruvian Interpolated Data of the SENAMHT's Climatological and Hydrological Observations. *Precipitación v1.0*.
- Li, M. and Shao, Q., 2010. An improved statistical approach to merge satellite rainfall estimates and rain gauge data. *Journal of Hydrology*, 385 (1–4), 51–64. doi:10.1016/j.jhydrol.2010.01.023
- Lindstr, J., et al., 2013. *Spatiotemporal: An R package for spatio-temporal modelling of air-pollution*. R package, 33.
- Lussana, C., et al., 2018. SeNorge2 daily precipitation, an observational gridded dataset over Norway from 1957 to the present day. *Earth System Science Data*, 10 (1), 235–249. doi:10.5194/essd-10-235-2018
- Ly, S., Charles, C., and Degré, A., 2013. Different methods for spatial interpolation of rainfall data for operational hydrology and hydrological modeling at watershed scale: a review. *Base*, 17 (2), 392–406. Available from: <http://popups.ulg.ac.be/1780-4507/index.php?id=10003%5Cnhttp://www.scopus.com/record/display.uri?eid=2-s2.0-84878998500&origin=inward&txGid=0>
- Mantas, V.M., et al., 2015. Validation of TRMM multi-satellite precipitation analysis (TMPA) products in the Peruvian Andes. *Atmospheric Research*, 163, 132–145. Elsevier B.V. doi:10.1016/j.atmosres.2014.11.012
- Manz, B., et al., 2016. High-resolution satellite-gauge merged precipitation climatologies of the Tropical Andes. *Journal of Geophysical Research: Atmospheres*, 121, 1190–1207. doi:10.1002/2015JD023788.Received



- Manz, B., *et al.*, 2017. Comparative ground validation of IMERG and TMPA 2 at variable spatio-temporal scales in the Tropical Andes. *Journal of Hydrometeorology*, 18, 2469–2489. doi:10.1175/JHM-D-16-0277.1
- Marengo, J.A., *et al.*, 2012. Recent developments on the South American monsoon system. *International Journal of Climatology*, 32 (1), 1–21. doi:10.1002/joc.2254
- Nerini, D., *et al.*, 2015. A comparative analysis of TRMM-rain gauge data merging techniques at the daily time scale for distributed rainfall-runoff modelling applications. *Journal of Hydrometeorology*, 150904104740009. doi:10.1175/JHM-D-14-0197.1
- Nesbitt, S.W. and Anders, A.M., 2009. Very high resolution precipitation climatologies from the tropical rainfall measuring mission precipitation radar. *Geophysical Research Letters*, 36 (15), 1–5. doi:10.1029/2009GL038026
- New, M., Hulme, M., and Jones, P., 2000. Representing twentieth-century space – time climate variability. Part II: development of 1901 – 96 monthly grids of terrestrial surface climate. *Journal of Climate*, 13 (13), 2217–2238. doi:10.1175/1520-0442(2000)013<2217:RTCSTC>2.0.CO;2
- Newman, A.J., *et al.*, 2015. Gridded ensemble precipitation and temperature estimates for the contiguous United States. *Journal of Hydrometeorology*, 16 (6), 2481–2500. doi:10.1175/JHM-D-15-0026.1
- Nicolas, J.P. and Bromwich, D.H., 2011. Precipitation changes in high southern latitudes from global reanalyses: a cautionary tale. *Surveys in Geophysics*, 32 (4–5), 475–494. doi:10.1007/s10712-011-9114-6
- Notivoli, R.S., *et al.*, 2017. *Reconstrucción e incertidumbre en series de precipitación diaria instrumental*. X Congreso Internacional AEC: Clima, Sociedad, Riesgos y Ordenación Del Territorio, 397–406.
- Ochoa, A., *et al.*, 2014. Evaluation of TRMM 3B42 precipitation estimates and WRF retrospective precipitation simulation over the Pacific-Andean Region of Ecuador and Peru. *Hydrology and Earth System Sciences*, 18 (8), 3179–3193. doi:10.5194/hess-18-3179-2014
- Parmentier, B., *et al.*, 2015. Using multi-timescale methods and satellite-derived land surface temperature for the interpolation of daily maximum air temperature in Oregon. *International Journal of Climatology*, 35 (13), 3862–3878. doi:10.1002/joc.4251
- Perdigón-Morales, J., *et al.*, 2017. The midsummer drought in Mexico: perspectives on duration and intensity from the CHIRPS precipitation database. *International Journal of Climatology*. doi:10.1002/joc.5322
- Peterson, T.C., *et al.*, 1998. Homogeneity adjustments of in situ atmospheric climate data: a review. *International Journal of Climatology*, 1517, 1493–1517.
- Rudorff, C.M., Melack, J.M., and Bates, P.D., 2014. Flooding dynamics on the lower amazon floodplain: 2. seasonal and interannual hydrological variability. *Water Resources Research*, 50 (1), 635–649. doi:10.1002/2013WR014714
- Saha, S., *et al.*, 2014. The NCEP climate forecast system version 2. *Journal of Climate*, 27 (6), 2185–2208. doi:10.1175/JCLI-D-12-00823.1
- Saha, S., Moorthi, S., and Pan, H.-L., 2010. The NCEP climate forecast system reanalysis. *Bulletin of the American Meteorological Society*, 91 (August), 1015–1058. doi:10.1175/2010BAMS3001.1
- Schuermans, J.M., *et al.*, 2007. Automatic prediction of high-resolution daily rainfall fields for multiple extents: the potential of operational radar. *Journal of Hydrometeorology*, 8 (6), 1204–1224. doi:10.1175/2007JHM792.1
- Sorooshian, S., *et al.*, 2000. Evaluation of PERSIANN system satellite-based estimates of tropical rainfall. *Bulletin of the American Meteorological Society*, 81 (9), 2035–2046. doi:10.1175/1520-0477(2000)081<2035:EOPSS>2.3.CO;2
- Stekhoven, D.J. and Bühlmann, P., 2012. MissForest — non-parametric missing value imputation for mixed-type data. *Bioinformatics*, 28 (1), 112–118. doi:10.1093/bioinformatics/btr597
- Strauch, M., *et al.*, 2016. Adjustment of global precipitation data for enhanced hydrologic modeling of Tropical Andean watersheds. *Climatic Change*, 1–14. doi:10.1007/s10584-016-1706-1
- Sun, Q., *et al.*, 2017. A review of global precipitation datasets: data sources, estimation, and intercomparisons. *Reviews of Geophysics*, 79–107. doi:10.1002/2017RG000574
- Teegavarapu, R.S.V. and Nayak, A., 2017. Evaluation of long-term trends in extreme precipitation: implications of in-filled historical data use for analysis. *Journal of Hydrology*, 550, 616–634. doi:10.1016/j.jhydrol.2017.05.030
- Teng, H., *et al.*, 2014. Estimating spatially downscaled rainfall by regression kriging using TRMM precipitation and elevation in Zhejiang Province, Southeast China. *International Journal of Remote Sensing*, 35 (22), 7775–7794. doi:10.1080/01431161.2014.976888
- Thouret, J.C., *et al.*, 2013. Combining criteria for delineating lahar-and flash-flood-prone hazard and risk zones for the City of Arequipa, Peru. *Natural Hazards and Earth System Science*, 13 (2), 339–360. doi:10.5194/nhess-13-339-2013
- Tozer, C.R., Kiem, A.S., and Verdon-Kidd, D.C., 2012. On the uncertainties associated with using gridded rainfall data as a proxy for observed. *Hydrology and Earth System Sciences*, 16 (5), 1481–1499. doi:10.5194/hess-16-1481-2012
- Ulloa, J., *et al.*, 2017. Two-step downscaling of Trmm 3b43 V7 precipitation in contrasting climatic regions with sparse monitoring: the case of Ecuador in Tropical South America. *Remote Sensing*, 9 (7), 758. doi:10.3390/rs9070758
- van Osnabrugge, B., Weerts, A.H., and Uijlenhoet, R., 2017. GenRE: a method to extend gridded precipitation climatology data sets in near real-time for hydrological forecasting purposes. *Water Resources Research*, 53 (11), 9284–9303. doi:10.1002/2017WR021201
- Vera, C., *et al.*, 2006. The South American low-level jet experiment. *Bulletin of the American Meteorological Society*, 87 (January), 63–77. doi:10.1175/BAMS-87-1-63
- Verdin, A., *et al.*, 2015. A bayesian kriging approach for blending satellite and ground precipitation observations. *Water Resources Research*, 1359–1371. doi:10.1002/2014WR015432.Received
- Vicente-Serrano, S.M., *et al.*, 2010. A complete daily precipitation database for Northeast Spain: reconstruction, quality control, and homogeneity. *International Journal of Climatology*, 30 (8), 1146–1163. doi:10.1002/joc.1850
- Vicente-Serrano, S.M., *et al.*, 2017. Recent changes in monthly surface air temperature over Peru, 1964–2014. *International Journal of Climatology*. doi:10.1002/joc.5176
- Wilks, D.S., 2006. *Statistical methods in the atmospheric sciences*. 2nd ed. WMO, 1994. *Guide to hydrological practices*. 5th ed. Geneva, Switzerland: World Meteorological Organization.
- Yanto, B.L., *et al.*, 2017. Development of a gridded meteorological dataset over Java Island, Indonesia 1985–2014. *Scientific Data*, 4, 170072. doi:10.1038/sdata.2017.72
- Yao, J., *et al.*, 2016. Annual actual evapotranspiration in Inland River catchments of China based on the Budyko framework. *Stochastic Environmental Research and Risk Assessment*. doi:10.1007/s00477-016-1271-1
- Yatagai, A., *et al.*, 2012. Aphrodite constructing a long-term daily gridded precipitation dataset for Asia based on a dense network of rain gauges. *Bulletin of the American Meteorological Society*, 93 (9), 1401–1415. doi:10.1175/BAMS-D-11-00122.1
- Zambrano-Bigiarini, M., *et al.*, 2017. Temporal and spatial evaluation of satellite-based rainfall estimates across the complex topographical and climatic gradients of Chile. *Hydrology and Earth System Sciences*, 21 (2), 1295–1320. doi:10.5194/hess-21-1295-2017
- Zubieta, R., *et al.*, 2015. Impacts of satellite-based precipitation datasets on rainfall-runoff modeling of the Western Amazon Basin of Peru and Ecuador. *Journal of Hydrology*, 528, 599–612. Elsevier B.V. doi:10.1016/j.jhydrol.2015.06.064
- Zulkali, Z., *et al.*, 2013. A critical assessment of the JULES land surface model hydrology for humid tropical environments. *Hydrology and Earth System Sciences*, 17 (3), 1113–1132. doi:10.5194/hess-17-1113-2013